Design and Implementation of an Orbitrap Mass Spectrometer Data Acquisition System for Atmospheric Molecule Identification

Wei Wang and Yongping Li *

Posted Date: 25 April 2023

doi: 10.20944/preprints202304.0922.v1

Keywords: data acquisition; Orbitrap mass spectrometry; spectrum analysis; FPGA; FFT analysis

Article

Design and Implementation of an Orbitrap Mass Spectrometer Data Acquisition System for Atmospheric Molecule Identification

Wei Wang [1,2,3,4], Yongping Li [1,2,3,4,*]

[1] National Space Science Center, Chinese Academy of Science, Beijing 100190, China
[2] University of Chinese Academy of Sciences, Beijing 100049, China
[3] Beijing Key Laboratory of Space Environment Exploration, Beijing 100190, China
[4] Key Laboratory of Science and Technology on Environmental Space Situation Awareness, Chinese Academy of Sciences, Beijing 100190, China
* Correspondence: lyp@nssc.ac.cn

Abstract: Orbitrap mass spectrometers have been widely used in environmental component analysis. This paper presents an enhanced data acquisition system for in-situ detection of Orbitrap mass spectrometry, which enables in-suit real-time signal processing and analysis for atmospheric molecules with small mass numbers.During previous space atmospheric explorations, quadrupole mass spectrometry (QMS) was usually utilized for analyzing isotopic compositions and complicated compounds in the mixture. However, the inevitable ion scattering and drift during mass transfer, as well as the QMS attenuator loss, result in a relatively lower signal-to-noise ratio of the produced mass spectrum. In recent years, a novel mass spectrometer, called an Orbitrap mass spectrometer, has been gradually accepted and used because of its non-destructive detection ability, high mass resolution, and accuracy. Nevertheless, Fourier transform ion cyclotron resonance mass spectrometry (FT-ICR MS) is preferred over the Orbitrap mass spectrometry for ground applications, especially for detecting low-mass components (e.g., below 50 atomic mass units) due to the former's superior resolution. As the mass number decreases, the detection system demands a higher sampling and processing rate. Additionally, in ground-based scenarios, mass spectrometry analysis software on computers is often employed to analyze the signals. Therefore, in order to achieve in-situ detection of the space atmospheric environment using the Orbitrap mass spectrometer, this paper proposes a real-time signal acquisition and processing system for mass spectrometry analysis. The system comprises of signal conditioning circuits, analog-to-digital conversion circuits, programmable logic circuits, and related software. These components perform spectrum analysis and process the signal in real-time on hardware components, allowing for high-speed acquisition and analysis of the signals produced by the Orbitrap mass spectrometer.

Keywords: data acquisition; Orbitrap mass spectrometry; spectrum analysis; FPGA; FFT analysis

1. Introduction

Mass spectrometry (MS) is a powerful analytical technique that has been widely used in various fields, such as proteomics, metabolomics, and environmental sciences, due to its high sensitivity, accuracy, and resolution. Mass spectrometry works by ionizing molecular composition and exciting corresponding electrical signals through high-voltage swept-frequency pulses [1]. By analyzing the frequency, pulse width, or waveform of the electrical signals, different atmospheric components can be identified. In recent years, the application of mass spectrometry in atmospheric analysis has attracted significant attention as it provides a comprehensive understanding of the chemical composition and transformation processes of atmospheric constituents. Atmospheric mass spectrometry detection generally focuses on detecting gases such as O_2 N_2, Rare Gases (e.g., He, Ne, Ar, Kr, Xe), H_2O, CO, CO_2, NO, NO_2 [2–4]. Here is some possible ingredients for mass range 1–50 as Table 1.

Preprints (www.preprints.org) | NOT PEER-REVIEWED | Posted: 25 April 2023 doi:10.20944/preprints202304.0922.v1

Table 1. possible ion for mass range 1–50.

mass	possible ion	mass	possible ion
1	H^+	27	HCN^+
2	H_2^+, D^+	28	N_2^+, CO^+, $C_2H_4^+$
3	HD^+, $^3He^+$	29	$^{13}CO^+$, $C^{17}O^+$, $^{15}NN^+$
4	He^+	30	NO^+
7	Li^+	32	O_2^+, SO_2^{++}
12	C^+	34	H_2S^+, $O^{14}O^+$
13	$^{13}C^+$	36	$^{36}Ar^+$, HCl^+
14	N^+, N_2^{++}	38	$^{38}Ar^+$, $^{37}HCl^+$
16	O^+, O_2^{++}, CH_4^+	39	K^+
17	OH^+, NH_3^+	40	Ar^+, Ca^+
18	H_2O^+	41	$^{41}K^+$
19	HDO^+, F^+	42	Kr^{++}
20	Ne^+, HF^+	44	CO_2^+, N_2O^+
22	CO_2^{++}, $^{22}Ne^+$	45	$^{13}CO_2^+$, $^{13}C^{17}OO^+$
23	Na^+	46	NO_2^+, $C^{18}OO^+$
26	$C_2H_2^+$	49	$H_2SO_4^{++}$

For the detection of atmospheric composition in aerospace, Quadrupole mass spectrometry is currently the most widely used mass spectrometry for atmospheric component detection [5]. However, due to the detection of ions in the quadrupole mass spectrometer being accomplished through collisions between ions and the detector, a significant loss of sensitivity may occur. Fourier transform mass spectrometry and orbitrap mass spectrometry are high resolution mass spectrometers. They can perform non-destructive testing and can achieve achieving higher accuracy and they are similar in the way they detect ions [6].

The motion of ions in an Orbitrap mass spectrometer can be classified into three types of resonant motion: radial, axial, and azimuthal. Radial motion refers to the oscillation of ions confined between the center electrode and the outer half electrode, with a frequency of w_{r} . Azimuthal motion is the rotational motion of ions around the center electrode, with a frequency of w_ϕ . Axial motion involves ions oscillating back and forth along the center electrode, also known as resonant motion, with a frequency of w_{z}. The axial frequency is independent of the initial velocities and coordinates of the ions and follows the Equation (1). The term k is related to the field curvature associated with the structure, and for a specific mass spectrometer, it is a constant that remains unchanged.

$$w_{\mathrm{z}} = \sqrt{k \cdot \frac{q}{m}} \tag{1}$$

The standard Orbitrap mass analyzer typically has a frequency range of 0.1–7 MHz for ions that are trapped with m/z in the range of 1–4000. The oscillation frequencies of common gas molecules in the atmosphere such as nitrogen, oxygen, and hydrogen, range from 0.8 MHz to 4.8 MHz [7].

Ideally, the current signal produced by an ion with a single mass number would resemble a sine wave. Its magnitude can be calculated using the following Equation (2). However, due to the presence of energy attenuation, it ultimately appears as an exponentially decaying sine wave. In situations where amplitude information is not of significant concern, or when the required sampling time is relatively short, it may be approximated as a sine wave.

$$I = -qNw\frac{\Delta z}{\lambda}\sin(w\mathrm{t}) \tag{2}$$

The weak current signal generated by the Orbitrap mass spectrometer needs to be linearly amplified before it can be collected by the data acquisition system. The operating voltage of the existing ADCs typically range from ±0.5 V to ±10 V, with the most common voltage range being

 doi:10.20944/preprints202304.0922.v1

±1 V to ±2.5 V. The current signal from the Orbitrap needs to be amplified to a voltage within the range of the ADC's operating voltage to be effectively detected without being overwhelmed by noise. The signal generated by the excitation of multiple gases is represented as a mixture of signals with different periods and amplitudes in the time domain [6]. The amplitude of the induced current is related to the number of molecules or atoms, and the current increases with the number of molecules or atoms. An existing amplifier circuit can be adapted for use in the Orbitrap by appropriately modifying the resistance and capacitance values [8]. Since this study focuses on the data acquisition system, it is assumed that the signal has been linearly amplified to a range of maximum ±5 V and minimum ±50 mV. After amplification, the system undergoes analog-to-digital conversion (ADC) and is processed by the corresponding controller to complete data acquisition and processing. Both Orbitrap mass spectrometry and Fourier transform mass spectrometry are demanding techniques that require a high-performance data acquisition system, characterized by good real-time performance and anti-interference capability. Such systems enable efficient acquisition and processing of high-quality mass spectral data, which are crucial for accurate measurement and analysis of complex molecular structures [9].Traditional data acquisition systems for OT-MS rely on computers, but with the development of modern electronic technology, digital signal processing systems based on Field-Programmable Gate Array (FPGA) technology are increasingly used in various fields, including data acquisition and processing [10]. The CORALS (Characterization of Ocean Residues And Life Signatures) mass spectrometer is designed for the exploration of liquid water, carbon-rich materials, and biomolecules on Jupiter's moon Europa. It is an Orbitrap mass spectrometer capable of detecting components with a mass range of 23–900 u. Despite the usage of a custom-made FPGA board for instrument control, no such board is involved in data acquisition nor utilized for Fourier transform spectroscopy in the instrument. Instead, other specially designed mechanisms and techniques are adopted to fulfill the data acquisition and Fourier transform requirements. The data acquisition process in the mentioned task is accomplished with the assistance of a National Instruments (NI) DAQ card. Meanwhile, the corresponding LabVIEW software is responsible for carrying out the fast Fourier transform (FFT) analysis [7]. Dayu Li developed a dedicated system with a high sampling rate of 12 Million samples per second (Msps) and a high accuracy of 14 bits. The system operates with an EP2C5Q208C8N FPGA and an ADS850 ADC, representing advanced hardware configurations. After the data acquisition stage, the digital signals are transmitted and further processed on a computer with appropriate software packages integrated [9]. FPGA-based data acquisition systems have the advantage of fast calculation speed, real-time performance, and anti-interference ability. FPGA real-time signal processing can be used to achieve rapid acquisition and processing of signals. Utilizing FPGA acceleration to implement preprocessing and conversion of mass spectrometry signals can improve the analysis speed and precision of mass spectrometry instruments. Additionally, the programmability and flexibility of FPGA technology can realize customized processing of mass spectrometry signals, completing modifications in aspects such as sampling, storage, control, etc,meeting the demands of different application scenarios [11–13]. Building on the foundations laid by previous researchers, a FPGA and ADC based data acquisition system that can analyze down to a mass-to-charge ratio of 2 is proposed. This system aims to distinguish the frequency and relative magnitude of the induced electric signal of atmospheric gas ions at mass numbers below 50, and analyze the mass spectrometry signal through Fourier transform analysis using FPGA. This system achieves real-time signal processing for mass spectrometry analysis for Orbitrap. In this article, we first discuss the main signal characteristics of Orbitrap. Furthermore, we will discuss the relationship between quality resolution, sampling rate, and the number of FFT points, making the requirements more explicit. Then we will make a detailed description of the designed system, including hardware design, signal processing algorithms, and data communication. To verify the system's performance, a series of experiments, including signal acquisition and FFT verification were conducted. The experimental results demonstrate that the designed data acquisition system effectively meets OT-MS's performance requirements in atmospheric detection. By simply modifying the sampling

Preprints (www.preprints.org) | NOT PEER-REVIEWED | Posted: 25 April 2023 doi:10.20944/preprints202304.0922.v1

rate and duration of sampling in the program, it is possible to achieve scenarios tailored to different resolution requirements.And this application of FPGA-based data acquisition systems in OT-MS offers a beneficial reference for data acquisition and processing in other spectrum analysis system.

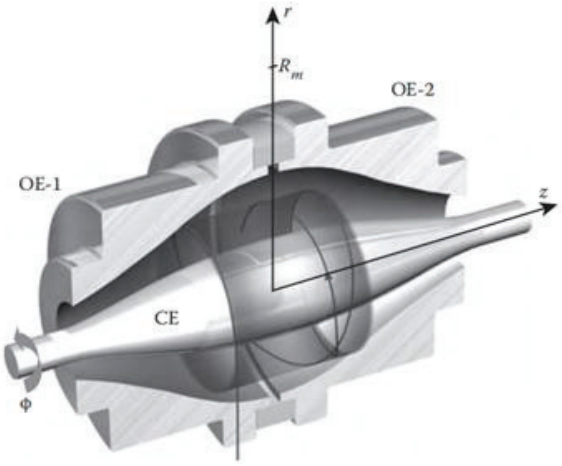

Figure 1. Orbitrap mass spectrum.

2. Related Work

In the measurement of signal frequencies, the frequency counting technique is commonly utilized; however, it is primarily suited suitable for measuring a single signal frequency. A different method involves using variable or multiple band-pass filters for multiple filtering to determine the frequency of the signal [14]. However, the implementation of this method presents significant challenges due to the wide frequency bandwidth required in the application scenario of this project. Therefore, this study utilizes the fast Fourier transform (FFT) method to decompose the signal into fundamental frequencies and multiple harmonics, thereby identifying potential frequency components of the signal [15]. The frequency resolution is dependent on the duration of signal collection, with higher resolution achieved through longer recording times but requiring greater storage capacity from the controller [16]. The expression for frequency resolution is given by: $\Delta f = f_s/N$. Where Δf is the frequency resolution, Hz; N is the number of points used for spectral resolution; and f_s is the sampling rate, Hz.

Analysis of periodic signals with finite length is equivalent to multiplying with a rectangular window in time-domain and convolution with a Sinc function in frequency-domain. When the two signals being measured satisfy the relationship as Equation (3), the main lobe region of the spectral graph centered on the two signals will not overlap, and both peaks can be distinguished completely [17].

$$|f_1 - f_2| > \frac{2}{T} \tag{3}$$

where f_1 and f_2 represent the frequencies of the two signals to be distinguished, Hz; and T is the duration of the signal, seconds.

When the two signals satisfy the relationship in Equation (4), their peaks will overlap to some extent, but they can still be distinguished. As the signal spacing decreases further, it will become increasingly difficult to distinguish two signals on the spectral graph.

$$\frac{1}{T} < |f_1 - f_2| < \frac{2}{T} \tag{4}$$

Signal can be fully restored if the sampling frequency satisfies the Nyquist sampling theorem—that is, the sampling frequency must be greater than twice the highest frequency in the signal; otherwise, aliasing will occur [18]. In practical engineering applications, the sampling rate is usually three to five times the highest frequency of the signal. In this study, we chose a sampling clock of 25 MHz.

Preprints (www.preprints.org) | NOT PEER-REVIEWED | Posted: 25 April 2023 doi:10.20944/preprints202304.0922.v1

For the gas component to be tested, we can draw from existing applications that the closest frequency interval is about 20 kHz [7]. In order to obtain a more accurate spectral graph and minimize overlap, the frequency resolution should be set to above 10 kHz when designing the spectral analysis system, that is, numerically less than 10 kHz according to Equation. At least 2,500 points are needed to achieve a resolution of 10kHz. Since the fast Fourier transform (FFT) algorithm decomposes a long sequence into operations with smaller numbers of points through butterfly operations [19], using the power-of-two-point calculation is more efficient. The selection of Fourier transform points is related to the logical resources available on the chip. In the field-programmable gate array (FPGA), the Block RAM (BRAM) is a relatively scarce resource. In situations that require high resolution, external storage can be utilized to achieve optimal resource utilization. For lower resolution requirements, internal BRAM can be employed to improve processing speed while maintaining resource optimization. Only ion components with a mass number below 50 are analyzed in this study, with a required frequency resolution that is not highly demanding. To meet the resolution requirements while preserving resources in the pre-research stage, we have chosen the FFT algorithm with 4096 data points. The decision was made with regard to the compromise between the desired resolution and the available resources. To ensure the fastest processing speed, SDRAM was not adopted, and only BRAM was used as the internal storage, achieving a frequency spectrum resolution within 7 kHz.

3. Design of the Acquisition and Processing System

3.1. System Architecture Design

The system designed for this study consists of both hardware and software components. The hardware aspect entails the signal conditioning and acquisition circuit, FPGA's main circuitry, and a serial-to-USB interface circuit. In contrast, the software focuses on the implementation of ADC driving and data acquisition, signal transformation using the Fast Fourier Transform (FFT) approach within the FPGA, establishment of the communication interface, and the display of information in the Matlab environment. The system architecture designed in this study is shown in Figure 2.

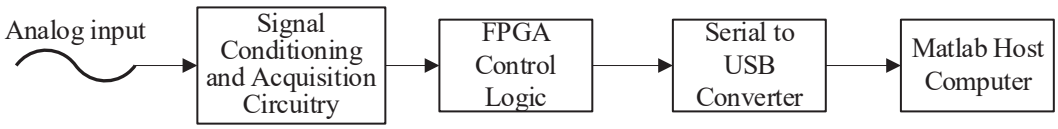

Figure 2. Overall structure block.

3.2. Hardware Design

3.2.1. Signal Conditioning Circuit

To limit the input range of the AD converter within the 1–3 V voltage supported by the ADC chip, an attenuation design for input voltage is needed . The signal conditioning circuit adopts AD8065 as an operational amplifier, which has the characteristics of high performance, low distortion, and high common mode rejection ratio, and is suitable for signal conditioning. The reference voltage, VREF, is provided by the ADC chip. The signal undergoes voltage following and voltage inverter by TL072U1, becoming NREF. After the signal from SMA undergoes resistive voltage divider, it enters the positive terminals of AD8065.And the negative input comes from NREF. The relationship between the output and input signals is as Equation (5).

$$V_{\text{out}} = \frac{1}{5} V_{\text{in}} + 2 \tag{5}$$

The output signal ADIN is connected to the ADC chip. The circuit diagram is shown in Figure 3. After signal conditioning,signals within plus/minus 5 V can be scaled to 1–3 V.

Preprints (www.preprints.org) | NOT PEER-REVIEWED | Posted: 25 April 2023 doi:10.20944/preprints202304.0922.v1

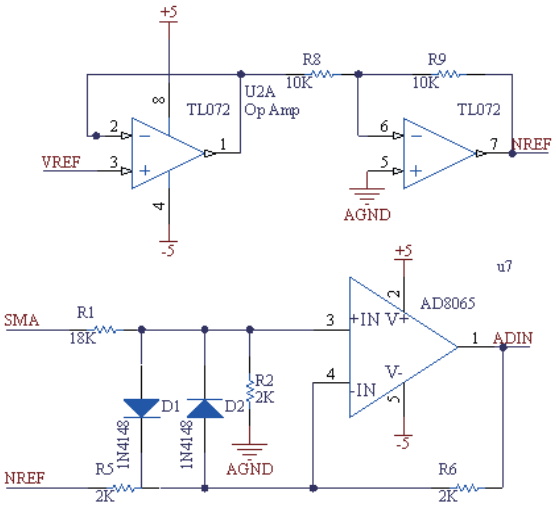

Figure 3. Signal condition.

3.2.2. Analog-to-Digital Conversion Circuit

we need to choose an ADC that meets the maximum sampling rate of greater than 25 M. The ADC chip we chose is the AD9226. It has the following features: it uses a single power supply and supports a maximum sampling rate of 65 MHz. The AD9226 chip internally integrates a high-performance sample and hold amplifier, which can maintain the accuracy of the input signal [20]. The chip adopts a multi-stage differential pipeline architecture, ensuring no code loss throughout the entire operating temperature range. The low noise and low distortion performance of AD9226 make it very suitable for data acquisition in this system. In this design, we configure AD9226 as single-ended mode and use the internal reference voltage of AD9226 to provide a stable and accurate voltage reference.

3.2.3. FPGA Control and Processor

The FPGA has been chosen as the core component for this signal processing system due to its ability to handle frequencies in the multi-megahertz range. After weighing cost and design considerations, the Intel EP4CE10F17C8 has been selected as the FPGA of choice. This device offers approximately 10K logic resources, 414 Kbit of BRAM, 46 multiplier resources, and 2 PLLs, effectively meeting the ongoing digital system design requirements of this project.

3.2.4. Serial-to-USB Interface Circuit

The CP2102USB is a widely-used USB-to-serial chip that offers fast transmission, low power consumption, high stability, and straightforward integration. This makes it an ideal choice for reliably converting the serial signal from the FPGA controller into a USB signal, which can then be transmitted to a computer for further analysis of frequency domain signals processed on the FPGA. The serial-to-USB converter circuit is shown in Figure 4 . The most important signals in serial communication are RXD and TXD. They respectively represent receiving data and sending data. D+ and D- respectively represent the positive and negative poles in the USB signal. When data is to be transmitted, the signal is divided into differential signals and transmitted to the connected device.

Preprints (www.preprints.org) | NOT PEER-REVIEWED | Posted: 25 April 2023 doi:10.20944/preprints202304.0922.v1

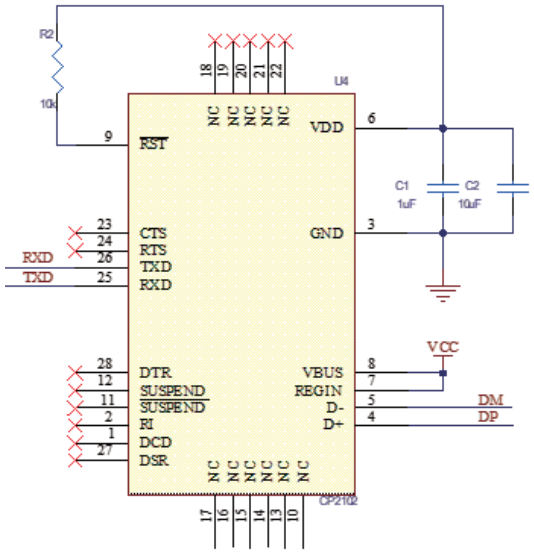

Figure 4. UART_to_USB circuit.

4. Software Design

This design is written in Verilog language, and the Quartus II 18.1 software is used as the running software. The design employs a modular structure that enables the instantiation of various functional modules within the field-programmable gate array (FPGA). Specifically, the signal is first sampled by an AD converter, which is driven by a clock, and then subjected to fast Fourier transform (FFT) for a predetermined number of points, resulting in the desired point results. Once the output meets the trigger signal, the data points are stored in the Random Access Memory (RAM) and transmitted to Matlab via a serial-to-USB interface circuit for advanced analysis and processing to obtain a spectrum. The process utilized is inherently fast, accurate, and well-suited to many signal processing applications. The overall signal flowchart is shown in Figure 5 .

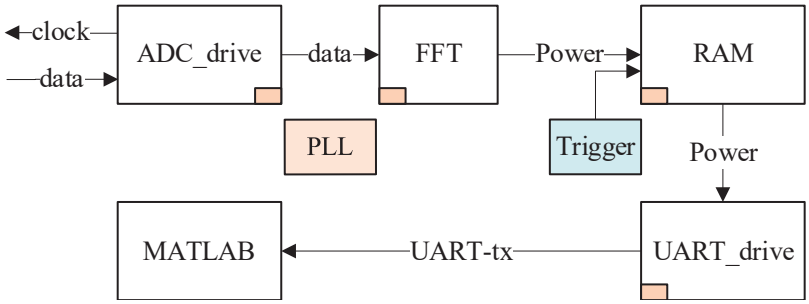

Figure 5. Software structure.

4.1. Clock Module

The PLL chip can achieve high-precision clock generation through its internal multiplication and division, as well as the use of an internal oscillator and feedback circuitry. The PLL mainly generates a high-precision 25 MHz clock for the ADC. The quality of the ADC clock affects the quality of signal sampling.

4.2. AD Acquisition Module

For AD9226, the data stored by the AD is acquired on the rising edge of the clock, and the acquired data is output through the data bus. The AD9226 requires no complex configuration. Under the 25 MHz clock period generated by the PLL, AD9226 can generate one sampling data per cycle. The collected data is in direct binary code, while the binary complement is usually used in the digital

Preprints (www.preprints.org) | NOT PEER-REVIEWED | Posted: 25 April 2023 doi:10.20944/preprints202304.0922.v1

signal processing algorithm of the FPGA, so corresponding conversion is necessary. After sampling begins, no valid data will be generated for up to approximately seven cycles. Note that there is some delay in the program.

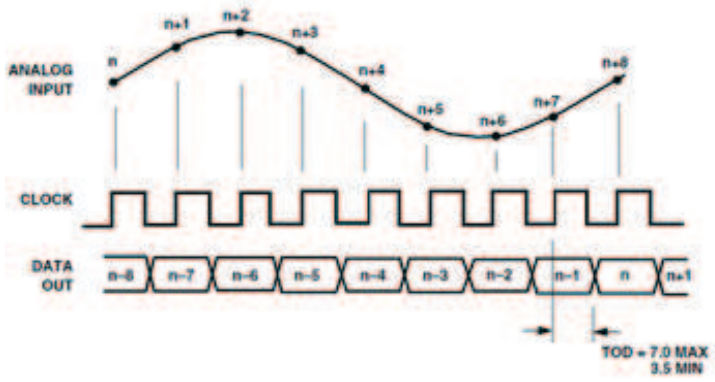

Figure 6. Timing diagram of AD9226.

4.3. Frequency Domain Analysis Module

The frequency domain analysis module, which encompasses the control module of FFT, FFT kernel, and amplitude spectrum module, is at the core of this design. This paper utilizes the FFT IP core provided by Intel to calculate the FFT of the input signal. The IP core boasts superb performance and low latency, supporting FFT and IFFT with 2 to the power of N points ($6 \leq N \leq 16$). Streaming mode can be continuously used to input data to the IP core for real-time dynamic detection requiring high response and refresh rates. In contrast, burst mode data flow format was used for mass spectrometry detection in this study because high data rate was required instead. The calculation result is output to the downstream module only after the data loading is complete.

The burst I/O data flow FFT is shown as Figure 7. The FFT control module is responsible for controlling the first and last input sink_sop and sink_eop provided to the IP core and determining the effective time sink_valid of the input signal. Additionally, it is in charge of generating the reset signal reset_n, as reported in [11]. Full-phase Fourier transform should be utilized when phase order needs to be considered for signals collected by AD. This design does not need phase information and therefore directly assigns the imaginary part of the input to FFT IP as 0 [21]. For the program design in this article, it is necessary to define a counting cycle signal that exceeds the sum of the FFT operation and delay time, which serves as a complete FFT cycle. Select the first and 4096th elements as sink_sop and sink_eop, respectively. Combine these control signals with the instantiated FFT IP core.

The output of FFT is also a complex signal, separated into real and imaginary parts. Due to the internal multiplication calculation by the IP core resulting in variation of bit width, an expansion of bit width would ultimately result in precision distortion. Floating point numbers require numerous resources for their exponents, hence block floating-point numbers are utilized in this calculation. In this case, a single data block shares one exponent, while the input data remains as fixed-point numbers, which guarantees superior signal-to-noise ratio and dynamic range throughout the entire operation process. The respective magnitudes of the real and imaginary signals obtained after the IP core produces the FFT result are then accordingly scaled, Take the top 12 bits as the result corresponding to the input twelve-bit signal. To prevent overconsumption of resources, a multiplier and adder are utilized in obtaining the corresponding 24-bit power spectrum after the squared sum of the real and imaginary parts is calculated. This avoids direct square root calculations inside the FPGA.

Preprints (www.preprints.org) | NOT PEER-REVIEWED | Posted: 25 April 2023 doi:10.20944/preprints202304.0922.v1

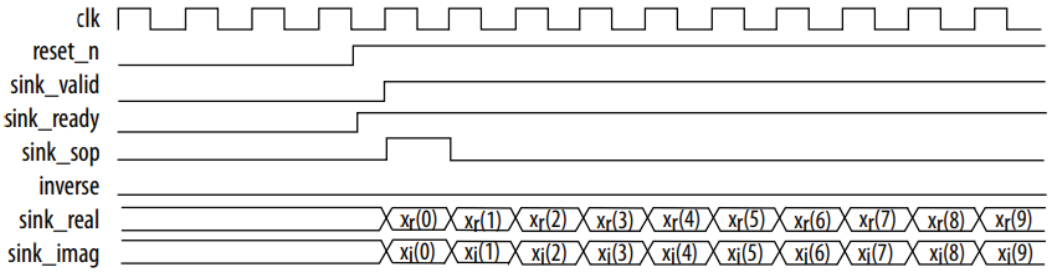

Figure 7. FFT timing block.

4.4. Storage and Communication Module

The selection of serial port RS232 for computer communication was based on the requirements of data volume and communication rate. Pseudo-dual-port RAM was utilized for data buffering to ensure that the data was read in the order of its corresponding amplitude. The RAM provides two access ports for reading and writing. Since the spectrum result has symmetry, only half the length of the FFT point number needs to be stored. The signal is divided into three bytes, and a state machine is designed to complete the transmission at different time points. Serial communication follows the RS232 protocol: a baud rate of 115200 with one start and stop bit and no parity bit.

4.5. Trigger Module

In mass spectrometry signal analysis, continuous spectrum monitoring is not necessary [22]. Therefore, only upon each button press, the storage and transmission module stores the corresponding point number after the next round of frequency domain analysis module is completed and transmits it through the serial port, thereby updating the frequency information of the signal.In subsequent practice, the button will be replaced by the signal for collecting and controlling the rocket or satellite sent out.

4.6. MATLAB-Based Upper Computer Method for Spectrum Graph Processing

The data sent by the FPGA is imported into the MATLAB serial tool for further processing. The incoming binary signal requires concatenation and binary conversion to retrieve the original 24-bit value. The value is then squared rooted and corrected by dividing the amplitude by the transformation point number N following the principles of Fourier transform. The abscissa of the frequency value can be obtained through Equation (6). Typically, spectral graphs are represented using logarithmic coordinates.

$$f = \Delta f \times n \ (n = 0 \sim \frac{N}{2} - 1) \tag{6}$$

4.7. The Overall Signal Flow in FPGA

The overall signal flowchart is shown in Figure 8.

Preprints (www.preprints.org) | NOT PEER-REVIEWED | Posted: 25 April 2023 doi:10.20944/preprints202304.0922.v1

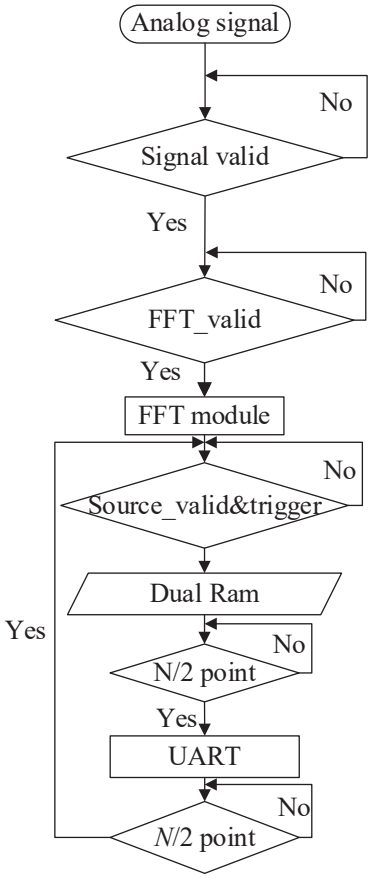

Figure 8. Signal logic.

5. Experimental Evaluation and Results

The ADALM2000 Multifunctional Module was used as the signal generator, and its corresponding changes were observed through the online debugging tool Signaltap in Quartus. Initially, the clock provided by the FPGA to the ADC was checked, and this verification is shown in Figure 9. It is evident that the generated clock signal is 25MHz as we use the main 50M clock to observe.

Figure 9. PLL test.

A DC voltage of 5 V was applied, and the acquired value of 2047 matched the expected value for a 5 V signal in a 12-bit AD system. Under the application of a direct voltage of -5 V, the measured values ranged from -1991 to -2048. This can be attributed to the inherent DC bias in the AD acquisition process, as well as the instability of the input voltage.

Next, a single-frequency 500k signal was applied to test the response of the AC signal. The acquired waveform takes 50 clock cycles under a 25M clock. The maximum value of the waveform was 2047. However, due to DC bias, the minimum value was -1985 as Figure 10. This error does not affect the frequency measurement.

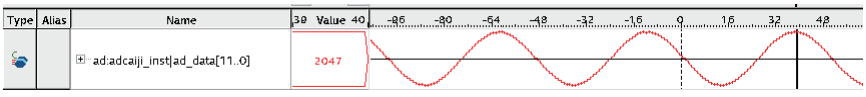

Figure 10. Sine_test.

Preprints (www.preprints.org) | NOT PEER-REVIEWED | Posted: 25 April 2023 doi:10.20944/preprints202304.0922.v1

The frequency spectrum of this single-frequency signal, which was not corrected for amplitude , is shown in the Figure 11. It is evident that the system recognizes the 500 kHz signal.

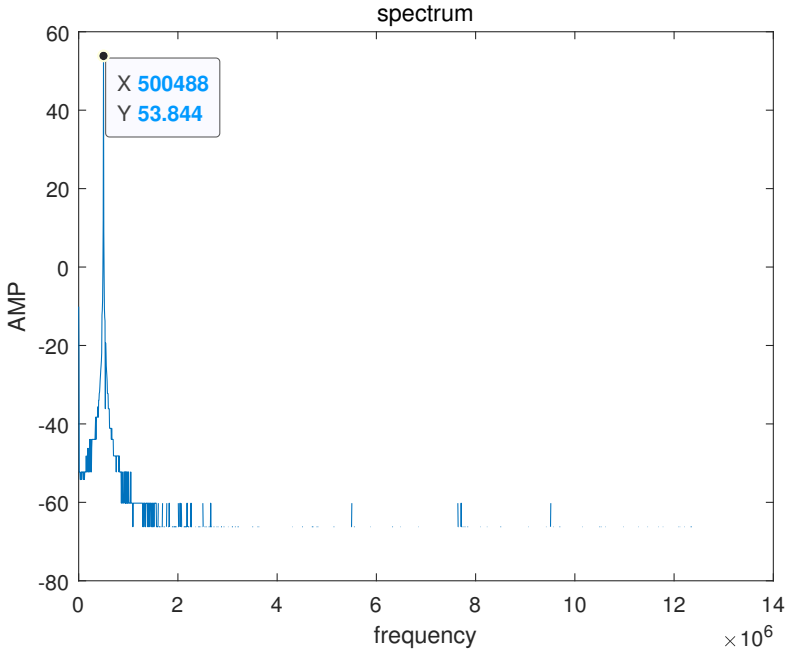

Figure 11. Sine_wave_frequency.

Next, the mixed frequency signal is tested by generating a composite signal of three different frequencies using a 8 bit DAC along with FPGA. FPGAs are capable of generating digital signals on their own. To produce test signals for this experiment, the Numerically Controlled Oscillator (NCO) IP core was employed to generate digital sine or cosine waveforms, which were subsequently converted into analog signals through a DAC module. The generated signals demonstrated high accuracy and stability, meeting the requirements of the experiment. In this experiment, three different frequencies were generated using the NCO IP core: 995 kHz representing Ozone, 1219 kHz representing Oxygen, and 4879 kHz representing Hydrogen. The signal generated at 995 kHz is adjusted twice the amplitude of the other two, and is used to verify the system's ability to determine amplitude. The AD9708 module outputs the mixed frequency signal, as shown in Figure 12, which satisfies the overall range of $+/-5$ V. However, useful information cannot be obtained in the time domain.

The spectrum analyzer in ADALM 2000 is utilized to analyze the generated mixed-frequency signal, and the corresponding spectral graph is shown in Figure 13, while the values of the peak points are shown in Table 2. The detected frequency signals of the acquisition system designed in this study were 995 kHz, 1221 kHz, and 4877 kHz as shown in Figure 14, while the results obtained using ADALM 2000 were 1001 kHz, 1221 kHz, and 4883 kHz. Since the frequency was not known in advance, there is a certain degree of spectral leakage, which can affect the measured frequency and amplitude. The measurement results of both methods had a certain error, but both were within 7 kHz of error and were mostly consistent with the theoretical spectral values, with correct line positions and similar spectral waveforms. The relative amplitude sizes also conform to the input test conditions. As the present experiment did not require extensive emphasis on amplitude information but only relative comparisons of amplitude, We did not perform much amplitude calibration.The current outcome of our study involves spectrum display.In the following practical project for space exploration, we will calibrate the system to ensure the reliability and accuracy of the data. By doing so, we will be able to determine the specific relationship between the spectrum and the mass spectrometric components, which will ultimately enable us to achieve complete mass spectrometric component analysis functions.

Preprints (www.preprints.org) | NOT PEER-REVIEWED | Posted: 25 April 2023 doi:10.20944/preprints202304.0922.v1

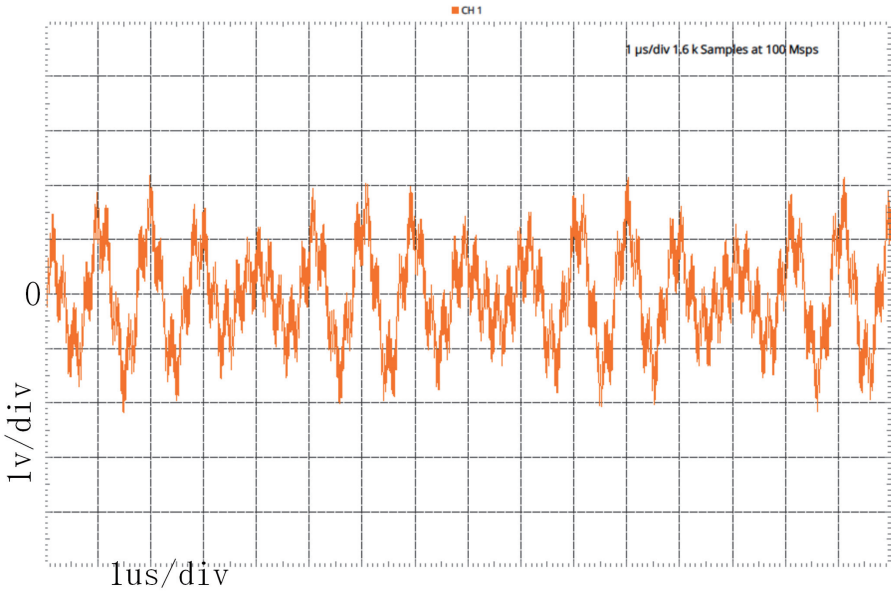

Figure 12. The generated mixed frequency signal.

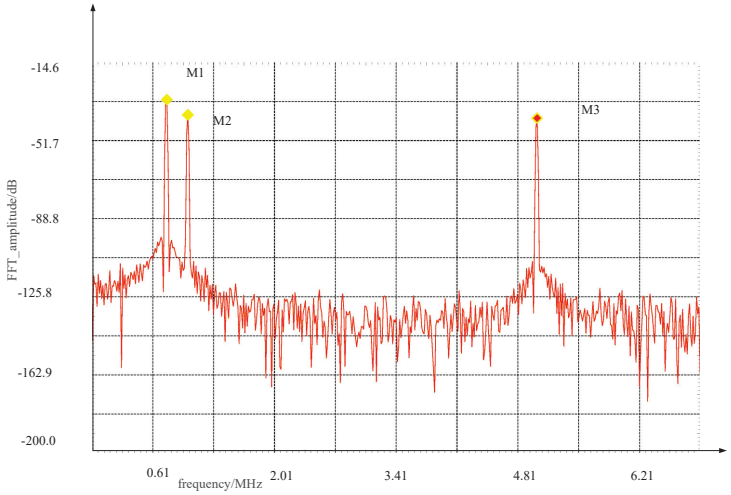

Figure 13. Result by ADALM2000.

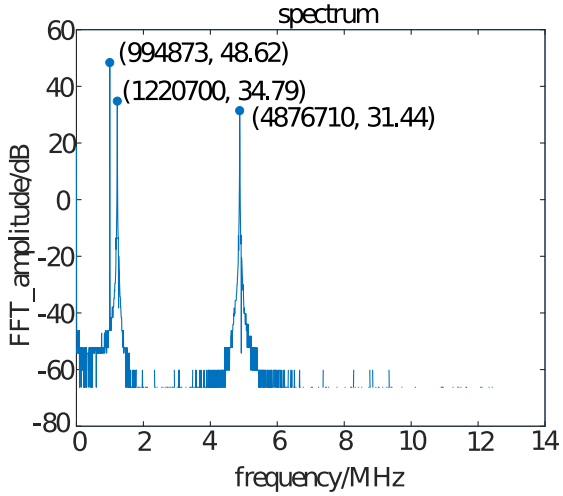

Figure 14. Result by designed system.

 doi:10.20944/preprints202304.0922.v1

Table 2. Result table.

Mark	Frequency/MHz	FFT_result /dB
M3	4.883	-37.6962
M2	1.221	-36.7333
M1	1.001	-32.3111

6. Conclusion

This article introduces a frequency analysis system for atmospheric mass spectrometry based on the AD9226 and FPGA. The data acquisition system, a low-cost solution with a conversion rate of 25M and precision of 12 bits, primarily performs signal conditioning and frequency analysis on the input signal to obtain spectral information of the measured signal. The system utilizes the high accuracy and fast conversion time of the ADC, and the high performance and low latency characteristics of the FPGA for FFT processing. In conclusion, our system has demonstrated its efficacy in conducting spectral analysis of atmospheric components with a mass number below 50. The system meets all design requirements and provides a feasible data acquisition solution for in-situ atmospheric sensing via orbittrap mass spectrometry. The effectiveness of this system has encouraged further development of orbit trap instrument detection systems. While the system has achieved its designed functions, there are still areas for improvement. For instance, the number of points used for Fourier transform can be adjusted to have variable point number to meet different resolution needs.When accurate quantification of atmospheric composition in Orbitrap mass spectral signals is necessary,better AD converters and detailed amplitude calibration should be employed.

Author Contributions: Wei Wang and Yongping Li; Formal analysis, Wei Wang and Yongping Li; Investigation, Wei Wang and Yongping Li; Methodology, Yongping Li; Software, Wei Wang; Validation, Wei Wang and Yongping-Li; Writing original draft, Wei-Wang; Writing review & editing, Wei Wang.

Funding: This research was funded by the Chinese Meridian Project, grant number Y91GJC15ES and grant number Y91GJC15DS.

References

1. De Hoffmann, E.; Charette, J.; Stroobant, V. *Mass Spectrometry: Principles and Applications*; 1997.
2. Von Zahn, U. Mass spectrometric measurements of atomic oxygen in the upper atmosphere: A critical review. *J. Geophys. Res.* **1967**, *72*, 5933–5937.
3. Herzog, L. Mass spectroscopy beyond the moon. *Int. J. Mass Spectrom. Ion Phys.* **1970**, *4*, 337–363.
4. Nier, A.O. Mass spectrometry in planetary research. *Int. J. Mass Spectrom. Ion Processes* **1985**, *66*, 55–73.
5. Ren, Z.; Guo, M.; Cheng, Y.; Wang, Y.; Sun, W.; Zhang, H.; Dong, M.; Li, G. A review of the development and application of space miniature mass spectrometers. *Vacuum* **2018**, *155*, 108–117. https://doi.org/10.1016/j.vacuum.2018.05.048.
6. Hu, Q.; Noll, R.J.; Li, H.; Makarov, A.; Hardman, M.; Graham Cooks, R. The Orbitrap: A new mass spectrometer. *J. Mass Spectrom.* **2005**, *40*, 430–443.
7. Willhite, L.; Ni, Z.; Arevalo, R.; Bardyn, A.; Gundersen, C.; Minasola, N.; Southard, A.; Briois, C.; Thirkell, L.; Colin, F.; et al. CORALS: A laser desorption/ablation orbitrap mass spectrometer for in situ exploration of Europa. In Proceedings of the 2021 IEEE Aerospace Conference (50100); IEEE: 2021; pp. 1–13.
8. Lin, T.Y.; Green, R.J.; O'Connor, P.B. A low noise single-transistor transimpedance preamplifier for Fourier-transform mass spectrometry using a T feedback network. *Rev. Sci. Instrum.* **2012**, *83*, 094102.
9. Li, D.; Fang, Y.; Huang, W.; Huang, X. Design and implementation of data acquisition system based on FPGA and USB interface in fourier-transform mass spectrometer. In Proceedings of the 2015 8th International Conference on Biomedical Engineering and Informatics (BMEI); IEEE: 2015; pp. 169–173.
10. Zieliński, M.; Chaberski, D.; Kowalski, M.; Frankowski, R.; Grzelak, S. High-resolution time-interval measuring system implemented in single FPGA device. *Measurement* **2004**, *35*, 311–317.
11. Uzun, I.S.; Amira, A.; Bouridane, A. FPGA implementations of fast Fourier transforms for real-time signal and image processing. *IEE Proc.-Vis. Image Signal Processing* **2005**, *152*, 283–296.

12. Mittal, S.; Gupta, S.; Dasgupta, S. FPGA: An efficient and promising platform for real-time image processing applications. In Proceedings of the National Conference On Research and Development in Hardware Systems (CSI-RDHS), 2008.
13. Sanaullah, A.; Yang, C.; Alexeev, Y.; Yoshii, K.; Herbordt, M.C. Real-time data analysis for medical diagnosis using FPGA-accelerated neural networks. *BMC Bioinform.* **2018**, *19*, 19–31.
14. Jiang, H.; Marpaung, D.; Pagani, M.; Vu, K.; Choi, D.Y.; Madden, S.J.; Yan, L.; Eggleton, B.J. Wide-range, high-precision multiple microwave frequency measurement using a chip-based photonic Brillouin filter. *Optica* **2016**, *3*, 30–34.
15. Sukhsawas, S.; Benkrid, K. A high-level implementation of a high performance pipeline FFT on Virtex-E FPGAs. In Proceedings of the IEEE Computer Society Annual Symposium on VLSI; IEEE: 2004; pp. 229–232.
16. Garrido, M.; Acevedo, M.; Ehliar, A.; Gustafsson, O. Challenging the limits of FFT performance on FPGAs. In Proceedings of the 2014 International Symposium on Integrated Circuits (ISIC); IEEE: 2014; pp. 172–175.
17. Hongwei, W. Fft basics and case study using multi-instrument. *Virtins Technol. Rev.* **2009**, *1*.
18. Landau, H. Sampling, data transmission, and the Nyquist rate. *Proc. IEEE* **1967**, *55*, 1701–1706.
19. Maslen, D.K.; Rockmore, D.N. The Cooley-Tukey FFT and group theory. *Not. AMS* **2001**, *48*, 1151–1160.
20. Analog Devices. *AD9226 Data Sheet*; 2001.
21. Shen, T.; Wei, L.; Zeng, X. Study on All-Phrase FFT Spectrum Analysis Technology in 25Hz Series Track Circuit Receiver. In Proceedings of the 2015 Information Technology and Mechatronics Engineering Conference; Atlantis Press: 2015; pp. 251–255.
22. Kumar, A.; Kumar, A.; Devrari, A. Hardware chip performance analysis of different FFT architecture. *Int. J. Electron.* **2021**, *108*, 1124–1140.